# TUNING AND PARAMETER OPTIMIZATION OF A DIGITAL INTEGRAL CONTROLLER FOR UNIFORM DROPLET SPRAY APPLICATIONS USING LEAD-FREE TIN-COPPER SOLDER

by

Eloisa M. de Castro

Submitted to the Department of Mechanical Engineering in Partial Fulfillment of the Requirements for the Degree of

Bachelor of Science

at the

Massachusetts Institute of Technology

[September]
June 2009





Signature of Author.....
Department of Mechanical Engineering
May 1, 2009

Certified by.....
Jung-Hoon Chun
Professor of Mechanical Engineering
Thesis Supervisor

Accepted by.....
John H. Lienhard
Professor of Mechanical Engineering
Chairman, Undergraduate Thesis Committee

TUNING AND PARAMETER OPTIMIZATION OF A
DIGITAL INTEGRAL CONTROLLER FOR UNIFORM DROPLET SPRAY
APPLICATIONS USING LEAD-FREE TIN-COPPER SOLDER

by

ELOISA MAE DE CASTRO

Submitted to the Department of Mechanical Engineering
on May 8, 2009 in partial fulfillment of the
requirements for the Degree of Bachelor of Science in
Mechanical Engineering

## Abstract

The advent of legislation restricting the use of lead in electronics requires innovation and refinement in processes for creating lead-free solder spheres for wafer bumping and other surface mount technology. Operation improvements were made upon a uniform droplet spray apparatus, and its digital integral controller was tuned for application to lead-free solder. Parameters determined included a range of initial controller command frequencies that would produce a stable image given a desired droplet diameter, and the value of the controller gain. The frequency range was determined by measuring the diameters of droplets attained at certain frequencies. The controller gain was optimized by measuring the time it took for the controller to reach its steady state at different gain values. It was determined that initial command frequency should be within ±150 Hz of that corresponding to the target diameter and an integral gain of 0.1 dB is the optimal gain for the tin-copper lead-free solder alloy, performing at par with the system specifications when in use with lead-bearing solder.

Thesis Supervisor: Jung-Hoon Chun
Title: Professor of Mechanical Engineering

# Table of Contents

## Acknowledgements

I would like to thank my thesis supervisor, Professor Jung-Hoon Chun, on whose unwavering patience, superb guidance, and valuable feedback I relied throughout my research. I am grateful to AJ Schrauth, whose numerous insights have been critical in moving this project forward. Special thanks also go to Pat McAtamney and Dave Dow for their outstanding recommendations that saved me considerable time and effort. I kindly thank my dear friend Monica Chu, who proofread this document meticulously. Last but not least, I thank my parents, Laarni and Arnulfo de Castro, for all of the emotional and financial support they have provided during my years at MIT.

# 1 Introduction

Global demand for consumer electronics has become increasingly sophisticated. The growing need for mobility, functionality, and interconnectivity has pushed the electronics market toward smaller devices, higher data storage capacity, and faster processing speeds. These trends have brought about waves of innovation in electronics packaging, evolving the standard from perimeter-style packages to area arrays. Area array packaging delivers top performance at the highest density, therefore making it fundamental to the miniaturization of these portable consumer devices [1].

Other benefits of area array packages include thermal management, applicability to multichip packages (MCPs), built-in solder connections, self-centering alignment, and high assembly yields. Ball grid arrays (BGAs), chip scale packages (CSPs), and flip chips (FCs) are modern area array packages in which balls of solder serve as electrical and mechanical connections between system levels. These solder balls are deposited onto a substrate, usually a silicon chip or wafer, in a grid-like bump pattern. **Figure 1** below is a schematic of a basic solder bump arrangement.

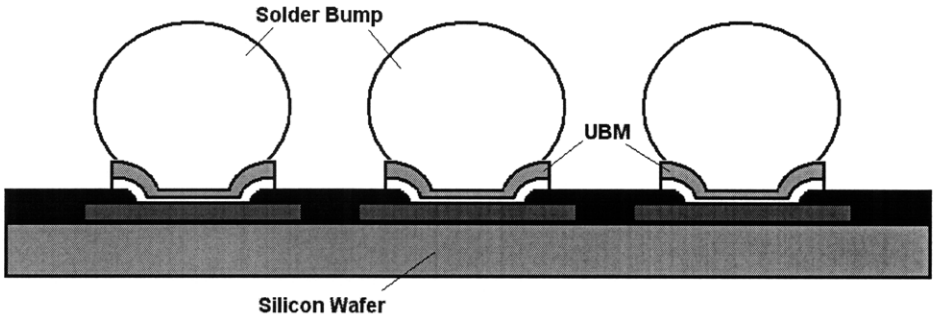


**Figure 1.** *Cross-Section of Solder Bumps on Silicon Wafer. Solder bumps are arranged in a dense grid pattern atop the under-bump metallurgy (UBM) of the wafer. Bump sizes can be as low as a few micrometers (μm) in height.*

The quality of these solder spheres is determined by their diameter, rotundity, and surface condition [2]. Uniform bump height is also essential to achieve the planarity needed for contact with the wiring board and form joints [1].

## 1.1 Solder-Bumping Processes

Common processes for solder bumping include evaporation, plating, stencil printing, and solder jetting [1,3]. In evaporation, metals are sputtered through a mask to form the under-bump metallurgy (UBM), and subsequently another, usually larger, mask is used to evaporate the solder [4]. The solder is then reflowed to achieve a smooth, spherical shape [1]. This technique is appropriate for high-temperature processing and is best-suited for solders with a high lead content [3]. Plating involves the conversion of metal salts into metals, and is a low-cost approach to solder bumping. Energy for this reaction is derived from either electric current or chemical reactions [1]. The primary difficulty with this method is irregular bump height [3]. Stencil printing, which is also less costly than evaporation, involves using a perforated stencil to print solder paste onto the under-bump metallurgy of the wafer [1,3]. This bumping method is very popular for most chip types, but not for high-density chips [1].

Solder jetting is a process by which droplets of solder are propelled directly onto the grid locations of the wafer. It is capable of producing highly uniform bumps, with precision reaching ±3% of mean droplet size [3]. This method originated from uniform droplet spray (UDS) technology, in which electrically charged molten metal droplets of uniform size are generated by breaking a laminar jet of the metal in controlled intervals [5]. The UDS process, which is also applicable to many types of droplet-based manufacturing (DBM), is illustrated in **Figure 2**.

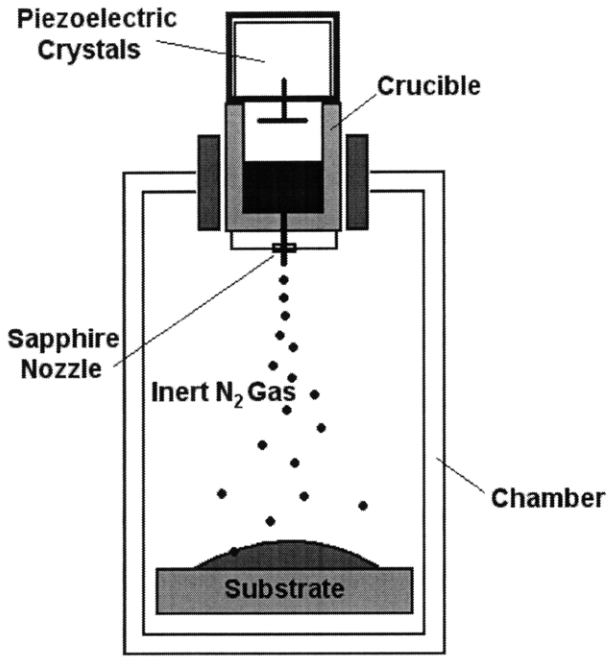


**Figure 2.** *The UDS Process. Vibrations within the mechanism break the jet flow and create droplets of uniform size.*

Droplet formation takes place within a nitrogen gas-filled chamber. The use of nitrogen gas or some other inert gas prevents oxidation of the solder. The solder is melted inside a crucible located at the top of the chamber. Once molten, the solder is flowed out through a precision-cut sapphire nozzle at the bottom of the crucible by applying an internal crucible pressure. A periodic impulse voltage is applied to piezoelectric crystals located above the melt. The crystals expand and contract repeatedly, disturbing the motion of the jet and causing it to break. The frequency at which these impulses are applied ultimately determines the size of the droplet.

Solder jetting technology balances precision with productivity; bumps can be created at speeds greater than 1000 bumps per second, and solder-jetting does not require the use of chemicals or stencils as with plating and printing [1]. With solder sphere production rates reaching up to 24000 balls per second [3], there is great potential for the high-volume application of this technology to expand in the future. The UDS process can be adapted for directly depositing solder droplets onto silicon wafers. For direct-deposition wafer bumping, droplets need not be electrically charged, and the substrate would be located closer to the nozzle exit for positional accuracy.

## 1.2 Electronics Lead Content Restrictions

Solder-bumping with tin-lead (Sn-Pb) alloys has been successfully implemented in the electronics packaging industry for over fifty years [3]. Recently, however, the environmental movement has led to legislation restricting the use of lead in the manufacture of electronics. The most influential such legislation thus far has been the Restriction of Hazardous Substances (RoHS) Directive, which was decreed by the European Union (EU) in February 2003 and became effective in July 2006 [6]. This mandate has presented the electronics packaging industry with difficulties, not only because of the lower supply and higher price of lead-free solder alloys, but also because of significant material differences between tin-lead alloys and their substitutes [1,6]. Most lead-free solders have higher melting points and are more prone to defects such as porosity, tin-whiskers and oxidation than their lead-containing counterparts [7].

The transition to lead-free electronics production requires that manufacturing processes designed for lead-containing solder be adapted to the new alloy's properties. Necessary modifications may include changing to materials that are more suited for higher operating temperatures and devising new packaging assembly techniques [6]. In processes compatible with lead-free solder, the execution parameters may still need altering because the process window, tolerance and margin of error are lower for lead-free than for Sn-Pb solder [8].

## 1.3 Solder Jetting in Lead-Free Applications

The electronics packaging industry was apprehensive of migrating to lead-free solder partly because of the limited amount of materials data available for non Sn-Pb soldering alloys [9]. Significant differences in material properties may require that certain equipment or substances used in the process be replaced. Solder jetting, however, has the advantage of needing very few changes for implementation in lead-free solder ball production despite material property variations. Furthermore, the performance of a solder jet is determined by the reliability of the machine's controller, so no new metal masks and chemicals are needed for a successful transition.

As shown in **Figure 3**, the UDS machine uses a controller that processes images of the droplets released from the crucible, then utilizes this feedback to adjust the vibration frequency of the piezoelectric crystals [10].

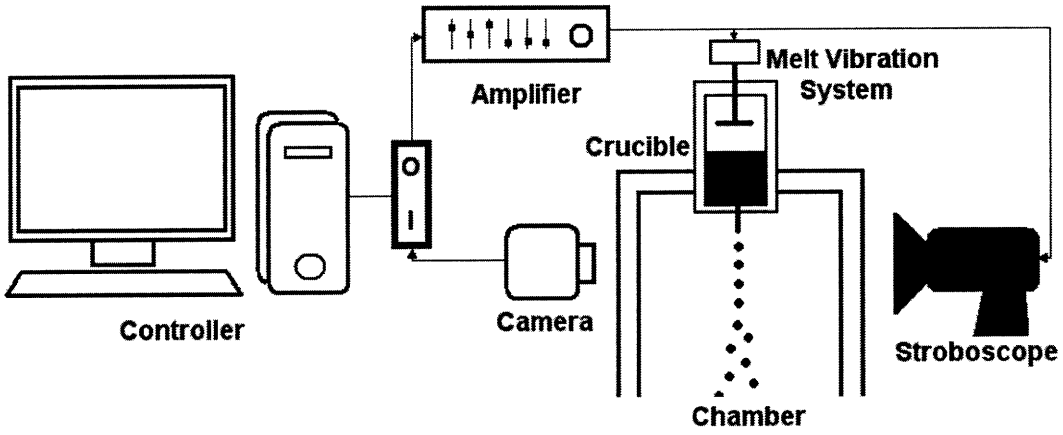


**Figure 3.** *Controller Loop of the UDS System. The droplets of interest are those most recently formed because drag and electric repulsion forces increase the error further down the chamber. Images of these droplets are gathered and analyzed to monitor the performance of the apparatus. The controller outputs a new frequency to compensate for the error measured. This signal is amplified then sent to the melt vibration system and the stroboscope simultaneously to compensate for the error and image the performance once again.*

This study explores and documents the effects of varying controller parameters on the performance of a digital integral controller designed for uniform droplet forming. Both the initial settings of the controller and the controller gain are varied to find the combination of parameters that results in the best controller performance.

# 2 UDS Controller

A closed-loop feedback control system has been created to control the UDS device. The droplet formation process is modeled under the assumption that the metal exits the nozzle as a continuous cylinder and is divided up into a series of shorter cylinders when the jet breaks [10]. **Figure 4** illustrates the breaking of a molten metal jet by repeated perturbation. Due to surface tension, these cylinders eventually reshape into a series of spheres of equal volume.

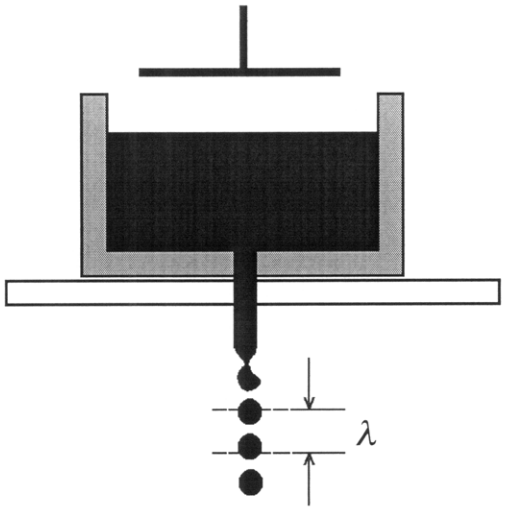


**Figure 4.** *Schematic of Jet Break-up. The jet is broken up into cylinders, which eventually form into spheres due to surface tension. The volume of the sphere is assumed to be the same as that of the cylinder, and the controller calculates ball diameter accordingly. The wavelength $\lambda$ is determined by finding the distance between sphere centers. The volume of the sphere is hence equal to the wavelength multiplied by the area of the orifice.*

Application of the Bernoulli principle describes the resulting ball diameter $d$ as a function of the fluid's densities in the solid $\rho_s$ and liquid $\rho_l$ phases, the orifice diameter $d_o$, the orifice coefficient of discharge $c_n$, the pressure difference $p$ between the chamber and crucible, the height $h$ of the melt within the crucible, gravitational acceleration $g$, and the frequency $f$ at which the jet is separated:

$$d = \left(\frac{9}{2}\frac{c_n^2 d_o^4 \rho_l}{\rho_s^2}\right)^{1/6}\left(\frac{p+\rho_l g h}{f^2}\right)^{1/6} \tag{1}$$

Of the diameter-determining parameters in Equation (1), only $p$, $h$, and $f$ are variable during the droplet manufacturing process. The variables $p$ and $h$ are treated as disturbances and $f$ becomes the control output.

Substituting

$$c_0 = \left(\frac{9}{2}\frac{c_n^2 d_o^4 \rho_l}{\rho_s}\right)^{1/6} \tag{2}$$

and the input parameter

$$\xi = f^{-1/3} \tag{3}$$

into Equation (1) gives the simplification

$$d = c_0\left(p + \rho_l g h\right)^{1/6}\xi \quad . \tag{4}$$

Ideally, the frequency commanded by the controller will approach the frequency corresponding to the target diameter without large overshoot and fluctuations. An integral control algorithm was chosen for its simplicity and its ability to achieve zero steady-state error. Noting the linearized Jacobian of Equation (4) as $y(k)$ and using the variable $u$ to denote the change $\Delta\xi$ in the input parameter, the digital integral controller can be represented as:

$$u(k+1) = u(k) - KT \cdot y(k) \quad , \tag{5}$$

where $K$ is the integral gain, and $T$ is the sampling time.

The asymptotic stability requirement for this control system has been evaluated to be

$$0 < KT < \frac{2}{c_0\left(p_i + \rho_l g h_i\right)^{1/6}} \quad , \tag{6}$$

where the subscript $i$ indicates the initial state of the melt. This sets a limit on the magnitude of the gain, given a certain sampling period.

The value on the right-hand side of Equation (6) increases with the material's solid-to-liquid density ratio,

$$\frac{\rho_s}{\rho_l} \, . \tag{7}$$

In previous applications with lead-bearing solder, the UDS controller has been shown to stabilize within 5 seconds. It is thus desirable for these specifications to be fulfilled in lead-free production. The lack of available materials property data on the lead-free alloy requires that the optimal gain setting be found experimentally. Increases

in gain allow the system to reach its target output more quickly yet introduce instability into the system through overshoot [11]. The ideal parameters should minimize the controller response time without risking instability.

The method through which feedback is obtained also influences controller performance. For the camera images to be analyzed properly, the droplets must exhibit uniform and stable jet break-up. This is achieved under the condition that the dimensionless growth factor of the solder is at least 0.8 [10]. The dimensionless growth factor is given by

$$\frac{q}{\sqrt{\rho_l d_0^3}} \tag{8}$$

where $q$ is the Rayleigh growth factor. This value quantifies the contraction of the jet's neck. The constraint satisfying the growth factor requirement was found to be:

$$\left(\frac{\lambda_{\min}}{v_{J\min}}\right)^{1/3} - \xi_i \le u(k) \le \left(\frac{\lambda_{\max}}{v_{J\max}}\right)^{1/3} - \xi_i \quad , k = 0,1,2,... \tag{9}$$

where $v_J$ is the velocity of the jet, and can be found using Bernoulli's principle. The subscript $i$ indicates the initial condition of the system. The nominal input determined from the model should be

$$\xi_i = \frac{d_t}{c_o(p_i + \rho_l g h_i)} \quad , \tag{10}$$

where $d_t$ is the target diameter. This input is equivalent to a nominal frequency of

$$f = \frac{\sqrt{c_0(p_i + \rho_l g h_i)}}{d_t^3} \quad . \tag{11}$$

The condition in Equation (9) above states that the commanded frequency must be within a certain range of frequencies in order for the controller to receive valid feedback images and work properly. Because the material properties that influence these constraints are undocumented, the parameters fulfilling these conditions must be found experimentally.

# 3 DBM Machine

The DBM machine consists of a vertical vacuum chamber that is sealed at its ends by two metal plates. **Figure 5** is a comprehensive diagram of the system. Attached to the top plate is a crucible into which bars of solder are inserted for melting. The chamber of the DBM machine must first be purged of oxygen so that the melted solder does not form an oxide stream as it exits the crucible [5]. This is accomplished with a mechanical vacuum pump attached to the bottom of the chamber. The chamber is then filled with nitrogen or some other inert gas supplied from a pressurized gas tank.

The crucible is heated to a temperature at or above the solder's melting temperature. Nitrogen gas is then released into the crucible to push the melt out through a precision-cut sapphire nozzle. The melt vibration system sends pulses through the melt and the jet is broken at even intervals, forming droplets of equal size. A stroboscope behind the droplets simultaneously flashes at the same command frequency as the melt vibration system. A camera in front of the device captures images of the droplets at the point of break up. The user sets the target diameter, adjusts the frequency to find a stable image, then runs the controller. The controller analyzes these images and outputs the next command frequency until the desired sphere diameter is attained.

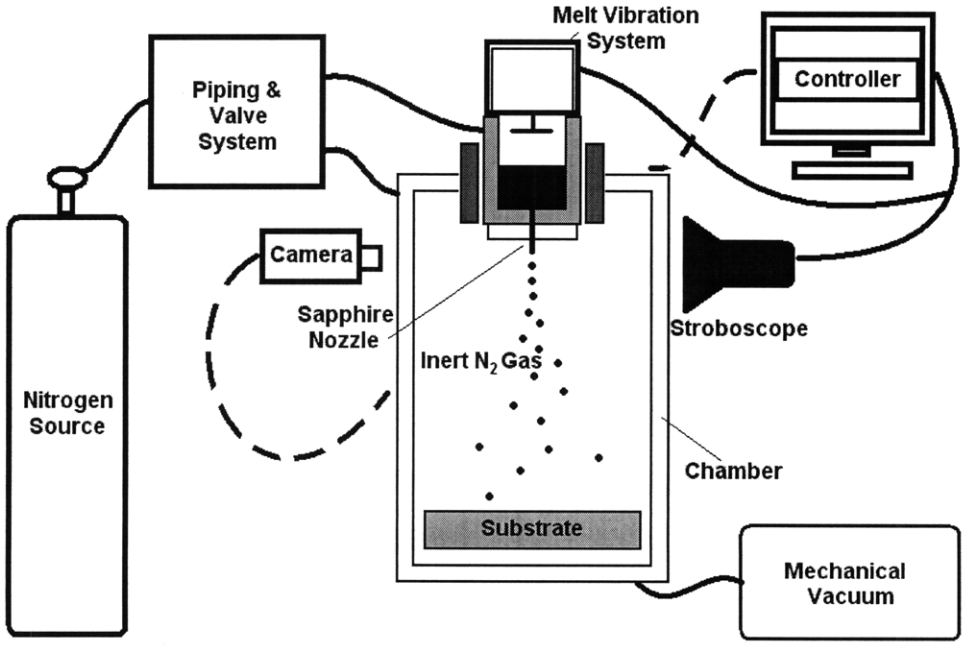


**Figure 5.** *The UDS System. The first step in the droplet production process is making the chamber inert. Next, the metal is melted and a jet stream is*

*formed. After the break-up of the jet is stabilized, the controller is activated to achieve the desired diameter.*

## 3.1 Machine Modifications

The following modifications have been made to the DBM machine in order to facilitate efficient experimentation:

i. The previous vacuum tube of 0.635 cm diameter was replaced by a high-density polyethylene tube of 2.54 cm diameter to accelerate the removal of oxygen from the chamber.

ii. A digital Allied Vision Technologies Guppy GF036B ASG camera replaced the former image-retrieving device and was mounted at a focal distance of 25.1 cm. The image plane is taken to be directly below the nozzle.

iii. A bottom plate with a larger, 2.54 cm vacuum orifice offset from the center was machined from 1.27 cm-thick Aluminum 6061 to promote efficient oxygen expulsion. The orifice was offset to eliminate the need for a substrate stand, as in previous applications of the machine. A screen was also put in place as a filter during oxygen expulsion.

iv. Digital high and low pressure gauges replaced the outdated dial-style pressure gauges. The 4-digit LCD readings had a ±1% accuracy and allowed for better control of the pressure difference between and chamber and crucible.

v. Piping was simplified. Only the connections to the chamber were made visible and rigid copper piping replaced polyethylene for permanent sections of the piping. Linkages between the plate and top plate were labeled for ease of assembly.

vi. The control panel was modified such that the instrumentation was arranged in an intuitive manner that followed the procedure. For example, all instrumentation used for making the chamber inert was grouped together. Extraneous devices such as a function generator and oscilloscope were removed.

vii. Procedures for running the DBM machine were revised.

# 4 Experimental Design

The controller gain and initial command frequency must be tuned while the machine is in production of solder spheres to determine optimal parameters. The DBM machine was run several times to obtain multiple data points.

## *4.1 Revised Procedures for Running the DBM machine*

1. The crucible plate is prepared by inserting a 150 μm sapphire nozzle into the cavity at the center of the plate. Regenerated cellulose film was be used to align the nozzle before adhering it to the crucible plate with high-temperature cement. The cement was allowed to cure.

2. 0.4 kg of lead-free Sn0.7Cu solder in bar form were inserted into the crucible and the crucible plate was bolted onto the crucible, with a graphite gasket to seal. The charging plate was attached and connected to the voltage source.

3. The top plate was bolted onto the top of the chamber such that the thermocouple and heater connections faced the front. Then the seven connections from the panel were attached to their labeled top plate counterparts.

4. Crucible and chamber relief valves were set pointing to "To Crucible" and "To Chamber" respectively. The high pressure valve was set to "Connect Chambers" and the low pressure valve to "Off."

5. The valve at the nitrogen gas source was opened. Low pressure was set to 35 kPa and high pressure to 80 kPa.

6. Oxygen was purged from the chamber by vacuuming it until the chamber pressure gauge indicated that the air inside the chamber has been removed. Chamber is filled with nitrogen by setting the low pressure valve to "On." Once the chamber pressure approached 35 kPa, the low pressure valve was set to OFF and air was purged from the chamber two more times.

7. Leaving the nitrogen on, the Control Power and the Heater Power were

switched on. The temperature controller was set to 300°C. The power supply and amplifier were also switched on.

8. In LabVIEW, the virtual instrument "Run UDS System.vi" was opened. LabVIEW contained image analysis programs that simplified the control process, hence the controller was programmed in LabVIEW.

9. The high pressure valve was turned on to set a jet in motion. The camera was focused at the section immediately after the transition from jet to droplets. Controller image settings such as brightness and shutter speed were adjusted to obtain an image that was easy to analyze. Frequency was adjusted until the image looked like a series of equally-spaced dots. **Figure 6** shows the user interface on the controller.

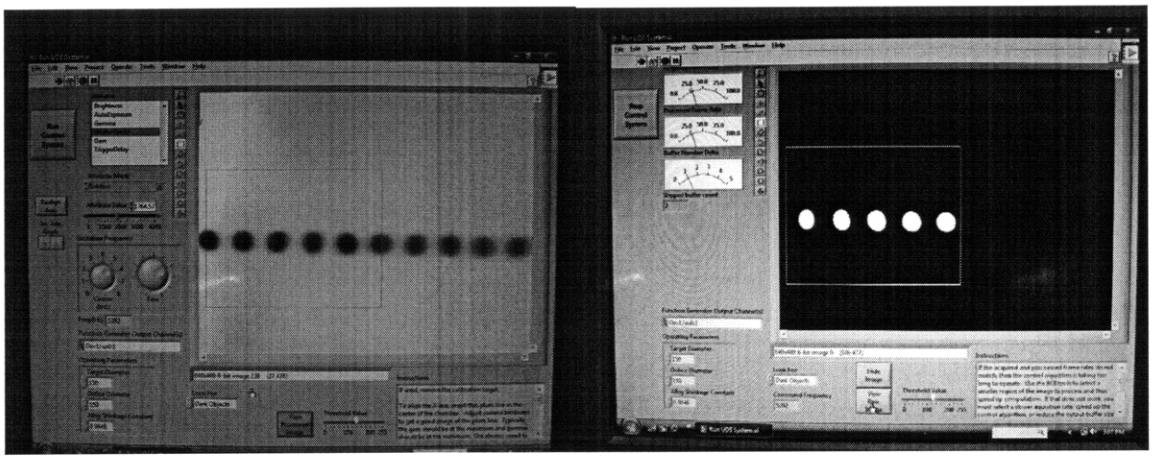

(a) (b)

**Figure 6.** *The LabVIEW User Interface. The interface allows the user to adjust image parameters such as brightness and shutter speed, and controller parameters such as frequency, target diameter and gain. The raw image shown in (a) is processed to look like (b). The processed image is simply a black and white version of the raw image where color is determined by comparing the pixel color in the raw image to a manually-selected threshold greyscale value for conversion to either black or white.*

## 4.2 Guaranteeing a Stable Image

The range of steady frequencies for the controller were found by running the machine and manually setting the frequency at which the melt vibration system was excited. The DBM was operated at pressures between 30.8 kPa and 45.6 kPa and the

controller gain was set to zero so that the frequency would not be altered during the run. The frequencies between 1000 Hz and 8000 Hz generating a stable image were recorded and spheres created during the run were gathered from the bottom of the chamber. Their diameters were measured by microscope and plotted against the frequency at which they were created. These spheres were produced through a nozzle of diameter 150μm.

These values were then compared with controller's diameter measurements to ensure that the controller was accurately measuring the diameters of the balls.

### 4.3 Optimizing Gain

In order to meet the 5-second stability previously achieved with lead-bearing solder, the controller's advance toward stability was timed for different values of gain. The DBM machine was operated at approximately 45.6 kPa and controller gains were varied between 0.01 dB and 0.5 dB. The time it took for the controller to stabilize was measured and recorded. The data was then used to determine the best gain value for the controller. Criteria for this included a settling time equal to or less than 5 seconds, and the absence of instability or overshoot during the run.

## 5 Results

The DBM experiments produced a collection of data that describing the behavior of the system. The outcome of these experiments is discussed in the following.

### 5.1 Stable Image Frequencies

It was found that the frequencies at which the best stable images were achieved were in the range of 3500 Hz – 6000 Hz. The frequency range differed if the difference between chamber and crucible pressure changed. An increase in pressure difference resulted in a higher outcome diameter at the same frequency. This corresponds to what was found in Equation (4). These results are displayed graphically in **Figure 7**.

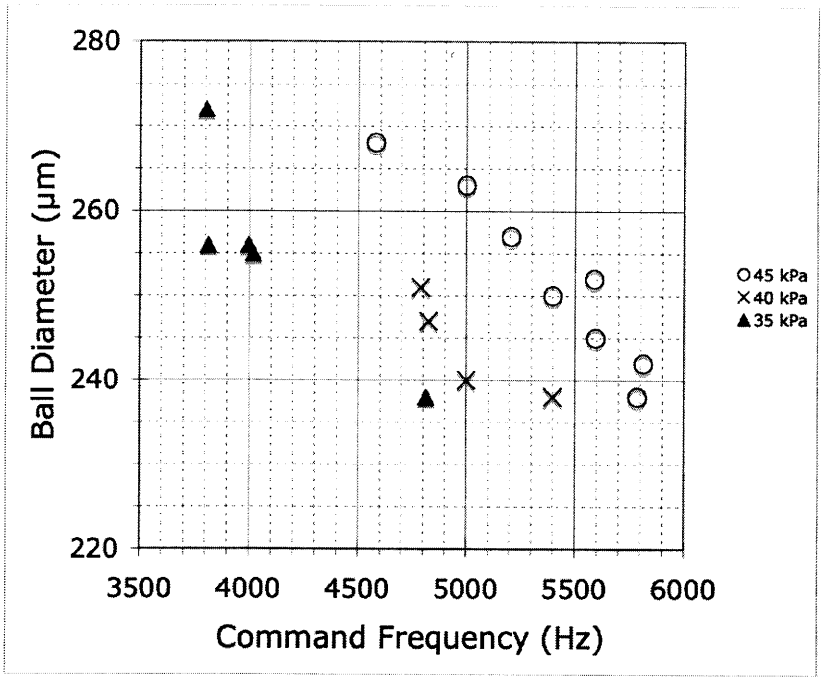


**Figure 7.** *The Correlation Between Frequency and Diameter. The diameter of the manufactured spheres has an inverse relationship with the command frequency, as predicted.*

The range of target diameters that could be obtained at a certain frequency varied by approximately 20 µm. For a given target diameter, the initial and commanded frequencies should remain within ±150 Hz of the expected frequency to maintain the stable image.

## 5.2 Controller Settling Times

The time it took for the controller to stabilize decreased from 0 dB to 0.1 dB, then increased as the gain surpassed 0.1 dB. Past a gain of 0.1 dB, the system appeared to overshoot its goal and oftentimes continued to move further away from the frequency that matched the target diameter. Only in rare cases was it able to reach the goal, and usually did not remain in the correct frequency range for long. **Figure 8** plots stability realization time against the applied controller gain. Gains showing a stability realization time greater than 60 seconds were not plotted.

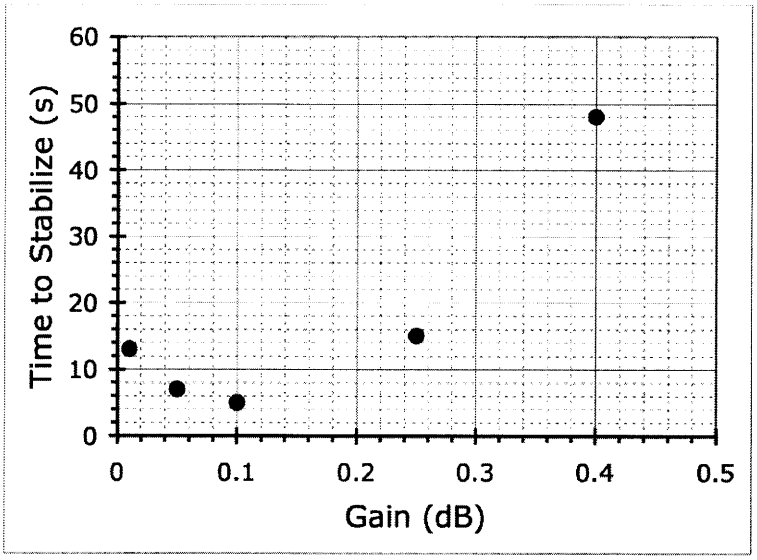


**Figure 8.** *Correlation Between Controller Gain and Time to Stability. The time to stabilize is at a minimum when the controller gain is 0.1 dB.*

# 6 Conclusion

This study has shown the optimal parameters under which the UDS controller should be operated for a 150 μm nozzle and Sn0.7Cu lead-free solder. Stable images occurred between frequencies of 3500 Hz and 6000 Hz, and the range of frequencies generating stable images differed in proportion to the pressure difference applied between the crucible and chamber.

The optimal gain for the controller was found to be 0.1 dB. This value results in a settling time of approximately 5 seconds, and matches the specifications of the system when under production of lead-bearing spheres. When gains are much greater than 0.1 dB, the controller spirals away from the ideal value and very rarely returns.

The results imply a range of 20 μm for possible final diameters produced by a given command frequency. Two disturbances that may cause this discrepancy are differing pressure differences between the crucible and the chamber and the change in height of the melt. Since the pressure difference was closely monitored during this run, the differences were likely due to the decreasing melt height within the crucible. This variation demonstrates how crucial a reliable controller is to the solder-jetting process.

The range of diameters created under the test conditions was between 235 μm and 275 μm, larger than the desired wafer bump height in most cases. Smaller orifice diameters can achieve the desired bump sizes. Also, there are many other lead-free solder alloys that may be applicable to solder jetting. This control process can be refined in the future for smaller nozzles and different lead-free alloys.

# References


[1] Gilleo, K., 2004, *Area Array Package Design*, McGraw-Hill, New York, NY.

[2] Gilleo, K., 2004, *Area Array Package Materials*, McGraw-Hill, New York, NY.

[3] Hsiao, W.-K., 2004, "Effects of Surface Properties on Solder Bump Formation by Direct Droplet Deposition," Massachusetts Institute of Technology, Cambridge, MA.

[4] Beddingfield, S.G., 2003, "Flip Chip Process Challenges for SMT Assembly," Electronic Packaging & Production, **43**(3), pp. 24.

[5] Passow, C.H., 1990, "A Study of Spray Forming Using Uniform Droplet Sprays," Massachusetts Institute of Technology, Cambridge, MA.

[6] Ganesan, S. and Pecht, M., 2004, *Lead-free Electronics*, John Wiley & Sons, Hoboken, NJ.

[7] Johnson, W., Lugo, R., Sattiraju, S.V., Jones, G., 2002, "Improving Lead-free Thermal Process Control," Nikkei Electronics Asia.

[8] Belmonte, J., 2005, "Step 2: Process Control," Surface Mount Technology.

[9] Pape, U. and Shulz, J.-U., 2006, "Characteristics of Lead-Free Solders During Flow Soldering (Selective and Wave Soldering)," *2006 Electronics Systemintegration Conference*, Dresden, Germany.

[10] Chun, J.-H., Rocha, J.C., Oh, J.-H., 2000, "Synthesis and Analysis of a Digital Droplet-Size Control System," Massachusetts Institute of Technology, Cambridge, MA.

[11] Ellis, G., 2004, *Control System Design Guide*, Elsevier Academic Press, Boston, pp. 98-110, Chap. 6.